Chemical Engineering Journal 352 (2018) 133–142

Contents lists available at ScienceDirect

Chemical Engineering Journal

journal homepage: www.elsevier.com/locate/cej

An acid-resistant magnetic Nb-substituted crystalline silicotitanate for selective separation of strontium and/or cesium ions from aqueous solution

Xudong Zhao[a,b], Qinghui Meng[b], Geng Chen[a], Zhihao Wu[a], Guangai Sun[c], Guobing Yu[d], Liusi Sheng[b], Hanqin Weng[a,*], Mingzhang Lin[a,e,*]

[a] Department of Engineering and Applied Physics, School of Physical Sciences, University of Science and Technology of China, Hefei 230026, PR China
[b] National Synchrotron Radiation Laboratory, University of Science and Technology of China, Hefei 230026, PR China
[c] Key Laboratory of Neutron Physics and Institute of Nuclear Physics and Chemistry, China Academy of Engineering Physics, Mianyang, Sichuan 621999, PR China
[d] Environmental Radiation Supervision Center, Environmental Protection Department of Anhui, Hefei 230071, PR China
[e] Institute of Nuclear Energy Safety Technology, Chinese Academy of Sciences, Hefei 230031, PR China

HIGHLIGHTS

- Magnetic Nb-CST, which can be separated easily by an external magnetic field, is able to eliminate Sr^{2+} and Cs^{+} at ppb level.
- Besides excellent selectivity towards Sr^{2+} and Cs^{+}, it is able to separate them from each other by adjusting pH.
- Even in real seawater, magnetic Nb-CST can remove as high as 94.19% of Cs^{+} at ppb level.
- Its high radiation stability and acid-resistance benefit the treatment of radioactive liquid wastes.

GRAPHICAL ABSTRACT

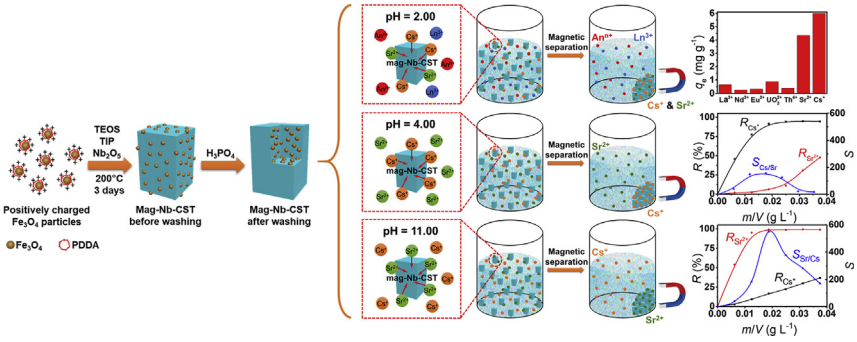

ARTICLE INFO

Keywords:
Magnetic adsorbent
Cesium
Strontium
Seawater purification
Radioactive liquid waste treatment

ABSTRACT

In this work, magnetic Nb-substituted crystalline silicotitanate (mag-Nb-CST), which can be used for separation of Sr^{2+} and Cs^{+} from aqueous solution, is successfully synthesized by embedding amine-functionalized Fe_3O_4 into the Nb-substituted crystalline silicotitanate (Nb-CST), being characterized by various techniques such as XRD, SEM, EDS, XPS, and VSM. The studies on the adsorption behaviors show that the adsorption process reaches equilibrium within about 8 h, and the maximum adsorption capacity on mag-Nb-CST is 14.38 mg g^{-1} at pH 11.00 for Sr^{2+}, and 11.18 mg g^{-1} at pH 4.00 for Cs^{+}, respectively. Besides the excellent selectivity towards Sr^{2+} and Cs^{+} over various lanthanides and actinides, the pH dependence on the adsorption capacity suggests a possibility to separate Sr^{2+} and Cs^{+} from each other by simply adjusting pH. Mag-Nb-CST is able to remove most of the Sr^{2+} and Cs^{+} at ppb level. Even in real seawater, it is able to remove 94.19% of Cs^{+}. Moreover, mag-Nb-CST shows good acid-resistance and radiation stability. The crystal structure and morphology remained almost the same after γ-irradiation with an adsorbed dose up to 435.8 kGy. Most importantly, only less than 0.1% of Fe is leached out from mag-Nb-CST at pH > 2, indicating that the embedded Fe_3O_4 nanoparticles are protected from corrosion by the coated Nb-CST, which is in favor of elimination of Sr^{2+} and Cs^{+} in acidic solutions. Thus,

* Corresponding authors at: Department of Engineering and Applied Physics, School of Physical Sciences, University of Science and Technology of China, Hefei 230026, PR China (M. Lin).
E-mail addresses: hanqinw@ustc.edu.cn (H. Weng), gelin@ustc.edu.cn (M. Lin).

https://doi.org/10.1016/j.cej.2018.06.175
Received 6 April 2018; Received in revised form 25 June 2018; Accepted 26 June 2018
Available online 28 June 2018
1385-8947/

mag-Nb-CST is a promising adsorbent in the treatment of acidic radioactive liquid wastes, and the purification of contaminated seawater.

1. Introduction

As nuclear power can provide efficient and relatively inexpensive energy with the minimum emission of carbon dioxide, it has been an important component of electricity generation in many countries. Nuclear power plants generated about 13.7% of the world's electricity in 2016 [1–3]. Treatment and management of spent nuclear fuels, generated from reactors, is an urgent problem. Accidents of uncontrolled release of radionuclides also received extensive attention. After Fukushima accident, about 630,000–770,000 tera-Becquerel radioisotopes were discharged into the environment, leading to environmental contamination in a large area [4,5]. Large amount of radioactive-contaminated water, containing ^{90}Sr, ^{134}Cs, ^{137}Cs and some other radionuclides, was also produced in the accident [6]. Radioactive Sr^{2+} and Cs^{+} are considered as principal sources of radioactivity and the highest safety risks in nuclear wastes, due to their high radioactivities and relatively long half-life times (28.79 years for ^{90}Sr, 2.06 years for ^{134}Cs and 30.2 years for ^{137}Cs) [7–10]. The chemical properties of Sr^{2+} and Cs^{+} in environment and biosphere are similar to potassium and sodium ions, which are water-soluble and easy to migrate. When radioactive Sr^{2+} and Cs^{+} enter human bodies, they may cause multiple diseases, such as carcinoma, cardiovascular disease, gastrointestinal distress, and so on [11–14]. So the removal of radioactive Sr^{2+} and Cs^{+} from water became an inevitable issue in radioactive waste disposal.

Among diverse methods applied in elimination of Sr^{2+} and Cs^{+} from water, adsorption is a simple, economical and feasible process which doesn't require complicated operating and equipment [15]. Various adsorbents including ferrocyanide, phosphomolybdate, and silicotitanate have been developed for adsorption and separation of Sr^{2+} and Cs^{+} from water in the past few decades. Among them, crystalline silicotitanate (CST) developed by Sandia National Laboratory (SNL) and Texas A&M University is a promising material for removing strontium and cesium due to its high adsorption selectivity, radiation stability, thermal stability and mechanical strength. Especially, CST is remarkable for its ability to separate cesium at parts-per-million concentration level from highly alkaline solution (pH > 14) containing high concentration of sodium (> 5 M) [16]. Although it was first synthesized for selectively removing cesium cations from aqueous solution [17], the uniform channels in its crystal structure were found to be ideally suitable for selective adsorption of strontium cations as well. The octahedrally coordinated structure of titanium atoms and tetrahedrally coordinated of silicon atom were proved to be responsible for the excellent selectivity towards Sr^{2+} and Cs^{+} [18]. An isomorphous substitution of CST was synthesized under hydrothermal conditions in 1996, whose titanium atoms in octahedral framework were partially replaced by niobium atoms [19,20]. Compared with unsubstituted CST, 25% niobium-substituted crystalline silicotitanate (Nb-CST) showed significantly higher uptake of Cs^{+} but lower uptake of Sr^{2+} [21]. The change in selectivity is caused by different coordination environments of Sr^{2+} and Cs^{+} in the channel, which were resulted from the variation on hydration sites in the tunnel [19,21,22]. The Nb-CST was commercialized by Universal Oil Products, named IONSIV® IE-910, but the Nb-CST particles were too small to be applied in column directly. Another commercial composite IONSIV® IE-911, in combination of Nb-CST powder and $Zr(OH)_4$ as binder, was developed to increase column performance [22]. However, Mann and Todd found that the $Zr(OH)_4$ binder in IONSIV® IE-911 was easy to be dissolved in acidic solution, which would degrade the performance of adsorption [23]. It has been a longstanding challenge to develop an acid-resistant adsorbent for practical application based on Nb-CST.

Besides column operation, magnetic separation is also widely used in practical wastewater treatment in the recent years, as magnetic adsorbents, being composites of adsorbent and magnetic nanoparticles, possess advantages of easy separation and short analysis time [24]. Varieties of Fe_3O_4 magnetic nanoparticles with different shapes and functional groups have been adopted in the preparation of magnetic adsorbents [25–28]. However, bare Fe_3O_4 tends to aggregate, causing the decrease in yield and adsorption efficiency of magnetic adsorbent. On the other hand, Fe_3O_4 is easy to be oxidized or corroded by acid, leading to the decrease in saturation magnetization [29].

In this work, we develop a simple method to synthesize magnetic Nb-substituted crystalline silicotitanate (mag-Nb-CST) by embedding amine-functionalized magnetic Fe_3O_4 nanoparticles into Nb-CST, which can be separated from water directly by external magnetic field. The mag-Nb-CST not only possesses excellent selectivity towards Sr^{2+} and Cs^{+} over various lanthanides and actinides, but also achieves the separation of Sr^{2+}/Cs^{+} from each other by adjusting pH. It is able to remove Sr^{2+} and Cs^{+} at ppb level, even in real seawater. Additionally, it has outstanding radiation stability and good acid-resistance, which make it possible to be applied in acidic solution. Thus, the mag-Nb-CST is promising in the elimination of Sr^{2+} and Cs^{+} from acidic radioactive waste treatment, and seawater.

2. Experimental sections

2.1. Materials

Strontium chloride hexahydrate ($SrCl_2{\cdot}6H_2O$, 99.5%), cesium chloride (CsCl, 99.5%), hydrochloric acid (HCl, 36–38%), phosphoric acid (H_3PO_4, 85%), hydrofluoric acid (HF, > 40%), sodium hydroxide (NaOH, 96%), ethylene glycol (99%), anhydrous sodium acetate (NaAc, 99%), 1,6-hexanediamine (99%), iron chloride hexahydrate ($FeCl_3{\cdot}6H_2O$, 99%) and alcohol (95%) were purchased from Sinopharm Chemical Reagent. Titanium isopropoxide (TIP, 97%) was purchased from Alfa Aesar. Poly dimethyl diallyl ammonium chloride (PDDA, average molecular weight: 200000–350000, ~20 wt% in water), tetrapropylammonium hydroxide (TPAOH, 2.0 M in water) and niobium oxide (Nb_2O_5, 99.9%) were purchased from Aladdin. Lanthanum chloride hexahydrate ($LaCl_3{\cdot}6H_2O$, 99.99%), neodymium chloride hexahydrate ($NdCl_3{\cdot}6H_2O$, 99.99%), europium chloride hexahydrate ($EuCl_3{\cdot}6H_2O$, 99.99%) and ethyl silicate (TEOS, 99%) were purchased from Energy Chemical. Cetyltrimethyl ammonium bromide (CTAB, 99%) was purchased from J & K Scientific. Standard reagent $UO_2(NO_3)_2$ ($1004 \pm 6\ \mu g\ mL^{-1}$) and $Th(NO_3)_4$ ($1000 \pm 4\ \mu g\ mL^{-1}$) were bought from Inorganic Ventures. Lead chloride ($PbCl_2$, 99%) was purchased from Shanghai No.4 Reagent & H. V. Chemical. All chemicals above were used without further purification. Seawater was collected from the Yellow Sea (north latitude 34.429611° and east longitude 119.574382°) and filtered with 220 nm cellulose esters membrane. Ultrapure water ($\rho = 18.25\ M\Omega\ cm$) was produced by ultrapure water polishing system purchased from Kertone Lab Vip®.

2.2. Synthesis of Fe_3O_4, Nb-CST and mag-Nb-CST

The Fe_3O_4 and Nb-CST were synthesized by adopting previously published methods [21,30]. A solution of 6.5 g of 1,6-hexanediamine, 2.0 g of anhydrous sodium acetate and 1.0 g of $FeCl_3{\cdot}6H_2O$ as a ferric source in 30 mL of glycol was stirred vigorously at 50 °C to give a transparent solution. The solution was transferred into a 50 mL Teflon-lined stainless-steel autoclave and reacted at 200 °C for 6 h. The Fe_3O_4 nanoparticles were rinsed with hot water and ethanol 3 times to remove

the solvent and 1,6-hexanediamine, then dried at 50 °C for 12 h [30]. The Nb-CST was synthesized by adding 1.72 g of titanium tetraisopropoxide, 1.67 g of tetraethyl orthosilicate, and 0.27 g of Nb_2O_5 to 25 mL of 3.3 M NaOH solution. The mixture was stirred for 1 h and then transferred to a 50 mL Teflon-lined stainless-steel autoclave reacting at 200 °C for 72 h. The resulting product was filtrated, rinsed with deionized water and ethanol, then dried at 65 °C overnight. The solid was exposed to 1 M HCl washing for three hours at room temperature to decompose the byproduct. The resulting solid was stirred in 1 M NaOH solution for 3 h at 40 °C to dissolve the amorphous constituents, then dried at 60 °C for 12 h [21].

The mag-Nb-CST was synthesized by dispersing 0.15 g of Fe_3O_4 and 0.32 g of Nb_2O_5 into 30 mL of 3.3 M NaOH and sonicated for 10 min, then added cationic surfactant (CTAB or PDDA), 2.06 g of titanium tetraisopropoxide and 2.00 g of tetraethyl orthosilicate into the suspension. The mixture was stirred for 1 h and then transferred to a 50 mL Teflon-lined stainless-steel autoclave and reacted at 200 °C for 72 h. A sample without cationic surfactant was also synthesized as a comparison. The resulting product was washed by the same method as Nb-CST. The bare Fe_3O_4 nanoparticles were washed away by exposing the resulting product to 1 M H_3PO_4 solution for 1 h at room temperature.

2.3. Investigation on stability of mag-Nb-CST

Radiation stability was studied by irradiating mag-Nb-CST with a Cobalt-60 γ source (30.4 kCi) for two absorbed doses, which are 108.9 and 435.8 kGy. The samples after irradiation were characterized by X-ray diffraction (XRD) and scanning electron microscopy (SEM) to analyze whether the crystal structure was damaged by radiation.

Acid-resistance was studied by dispersing 1.0 mg of mag-Nb-CST in 8 mL solution with different pH values (pH = 0, 1.00, 2.00, 4.00, 7.00, 11.00) for 3 days. The solution was filtered by 13 mm syringe filter with 0.22 μm cellulose membrane. The concentration of the leached Ti and Fe in the filtrates was analyzed by ICP-MS, which reflects acid-resistance of mag-Nb-CST to a certain extent. The total amount of Fe and Ti in the mag-Nb-CST was quantified by dissolving 20 mg mag-Nb-CST in 2 mL of 40% hydrofluoric acid solution, and then the concentration of metal ions was measured with ICP-OES after the solution was diluted 50 times with ultrapure water.

2.4. Adsorption of Sr^{2+} and Cs^{+} on mag-Nb-CST

Non-radioactive strontium (^{88}Sr) and cesium (^{133}Cs) were used instead of radioactive strontium (^{89}Sr) and cesium (^{137}Cs) in the adsorption experiments. The adsorption quantities for strontium, cesium, some lanthanides and actinides from aqueous solution on mag-Nb-CST were measured by a batch method at atmospheric pressure. All adsorption experiments were performed in polyethylene centrifuge tubes. The La(III), Nd(III), Eu(III), U(VI), Th(IV), Sr(II) and Cs(I) aqueous solutions with initial concentrations of 100 ng mL^{-1} were prepared. Then mag-Nb-CST was added and solid-to-liquid ratio was kept in the range of 3–1500 μg mL^{-1}. The pH value was adjusted by negligible volume of NaOH and HCl solution. The mixture was agitated for desired time at 80 rpm and 25 °C. The suspension was filtered by 13 mm syringe filter with 0.22 μm cellulose membrane after adsorption. The removal efficiency of Cs^{+} in seawater was investigated by the same procedures. The concentration of Sr^{2+} and Cs^{+} in the filtrate was analyzed by ICP-MS. The adsorbed quantity q_t (mg g^{-1}), equilibrium adsorbed quantity q_e (mg g^{-1}), removal efficiency R (%) and distribution coefficient K_d (mL g^{-1}) are determined using the following equations:

$$q_t = \frac{(c_0 - c_t) \times V}{m} \quad (1)$$

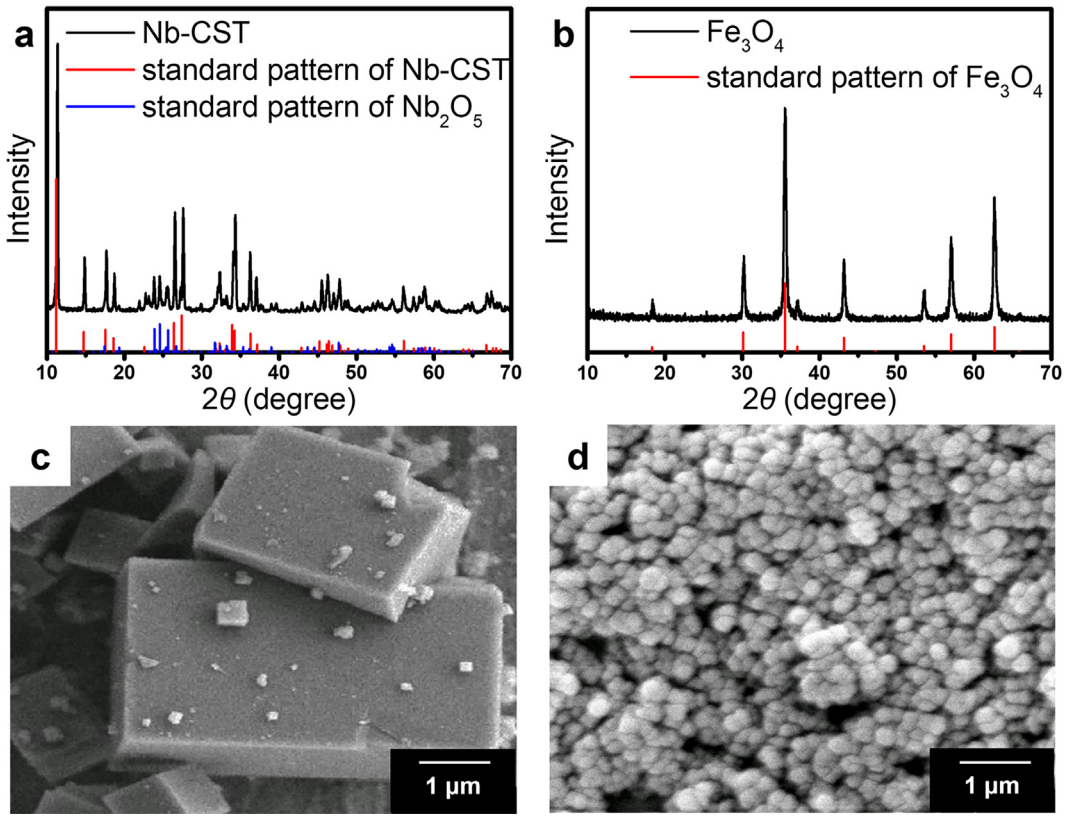

Fig. 1. XRD spectra of (a) Nb-CST, the red and blue lines are the indexed peaks from ICDD PDF 01-072-7604 (Nb-CST) and ICDD PDF 00-37-1468 (Nb_2O_5), (b) Fe_3O_4, the red line is the indexed peaks from ICDD PDF 00-11-0614 (Fe_3O_4). SEM images of (c) Nb-CST and (d) Fe_3O_4. (For interpretation of the references to colour in this figure legend, the reader is referred to the web version of this article.)

$$q_e = \frac{(c_0 - c_e) \times V}{m} \quad (2)$$

$$R = \frac{(c_0 - c_e)}{c_0} \times 100\% \quad (3)$$

$$K_d = \frac{(c_0 - c_e)}{c_e} \times \frac{V}{m} \times 1000 \quad (4)$$

where c_0 (mg L^{-1}) is the initial concentration of metal ions, c_t (mg L^{-1}) is the concentration of metal ions after adsorbing at the time t (min), c_e is the equilibrium concentration of metal ions, V (L) is the volume of the solution, and m (g) is the mass of adsorbent, respectively.

2.5. Characterization

Crystal structure of the samples was characterized by X-ray diffraction (XRD, Smartlab), which operated at 45 kV and 200 mA with Cu Kα radiation as the X-ray source (λ = 1.54178 Å), the step was set to 0.02°. The zeta potentials were recorded at different pH using a zeta potential instrument (Nano Brook 90 Plus PALS, Brookhaven) at 25 °C. The concentration of metal elements was analyzed by inductively coupled plasma mass spectrometer (ICP-MS, Thermo, X Series 2) using ^{185}Re or ^{115}In as internal standard and inductively coupled plasma optical emission spectrometer (ICP-OES, Optima 7300DV, PerkinElmer). Morphological characterization and elemental distribution were analyzed by cold field emission source scanning electron microscopy (cold FE-SEM, JEOL, JSM-6700F) at 10 kV with energy dispersive spectrometer (EDS, OXFORD INSTRUMENTS). Magnetic properties were studied by using a superconducting quantum interference device-vibrating sample magnetometer (SQUID-VSM) at room temperature. The XPS measurements were carried out with a spectrometer (ESCALAB 250, Thermo-VG Scientific) with Al Kα radiation (hν = 1486.6 eV, 200 W). The calibration of the energy was achieved by setting the major peak of C 1s at 284.6 eV.

3. Results and discussion

3.1. Synthesis and characterization of mag-Nb-CST

Nb-CST and Fe_3O_4 were synthesized by hydrothermal process at first. The XRD patterns of Nb-CST and Fe_3O_4 are shown in Fig. 1a and b, respectively, which are consistent with the diffraction from the (1 0 0), (1 1 3), (3 0 0) and (1 0 1) lattice planes of tetragonal Nb-CST (PDF#01-072-7604), and the diffraction from (3 1 1), (4 4 0), (4 0 0) and (4 1 1) lattice planes of cubic Fe_3O_4 (PDF#00-11-0614), respectively. The obtained Nb-CST particles are micron cubes (Fig. 1c), while Fe_3O_4 are spherical particles around 100 nm (Fig. 1d). Thus, it is possible to embed Fe_3O_4 nanoparticles inside Nb-CST, if Fe_3O_4 are added as seeds during the preparation of Nb-CST.

The pathway for synthesis of mag-Nb-CST is shown in Scheme 1. As-prepared Fe_3O_4, together with TEOS, TIP, and Nb_2O_5, was added in 3.3 NaOH solution, then mag-Nb-CST was prepared via the same hydrothermal process as Nb-CST. XRD pattern proves that mag-Nb-CST has been successfully synthesized (Fig. 1a). But since zeta-potentials of Nb-CST (−5.8 mV) and bare Fe_3O_4 (−14.9 mV) were both negative in 3.3 M NaOH solution, electrostatic repulsion between them resulted in low yield of mag-Nb-CST, which was only 51.6% (based on Ti [21]). So positively charged surfactants including CTAB, TPAOH, and PDDA were used to change the surficial charge of Fe_3O_4, turning electrostatic repulsion between Nb-CST and Fe_3O_4 into electrostatic attraction. The surfactants have different effects on the preparation of mag-Nb-CST. Addition of CTAB hindered the formation of Nb-CST (Fig. 2a), while TPAOH and PDDA didn't impeded the crystal growth process of Nb-CST (Fig. 2a and b). Moreover, with the addition of TPAOH and PDDA, the yields of mag-Nb-CST greatly improved to 74.0% and 84.0%, respectively. Mag-Nb-CST synthesized in presence of PDDA was used in other experiments due to its higher yield.

The embedding of Fe_3O_4 in Nb-CST was also verified by the SEM image (Fig. 2c). Both Nb-CST (Fig. 1c) and mag-Nb-CST (Fig. 2c) are micron cubes, implying that surfactant PDDA doesn't affect the morphology of the Nb-CST. For removing impurities, the as-prepared mag-Nb-CST was washed by phosphoric acid, hydrochloric acid and sodium hydroxide solution in sequence. XRD patterns of mag-Nb-CST before and after washing are shown in Fig. 2b. The disappearance of the peaks at 19.33, 20.43 and 20.84° indicates that most byproducts (such as natisite) have been removed. Characteristic peaks of Nb-CST and Fe_3O_4 still remain in the pattern of mag-Nb-CST after washing. Compared with mag-Nb-CST before washing, it is evident that all the Fe_3O_4 nanoparticles embedded on the surface of Nb-CST have been washed away (Fig. 2d). However, Fe still exists inside mag-Nb-CST after washing, according to the results of EDS (Fig. 2e and f). Based on the results of EDS and XRD, it can be concluded that Fe_3O_4 is dispersed not only on the surface, but also inside the mag-Nb-CST.

The magnetic properties of Nb-CST and mag-Nb-CST were also assessed at room temperature. Nb-CST, with an extrapolated saturation magnetization value of nearly 0 emu g^{-1}, was non-magnetic itself. With the addition of Fe_3O_4, mag-Nb-CST exhibited super-paramagnetism at room temperature. The extrapolated saturation magnetization values of mag-Nb-CST before and after washing were 10.22 and 5.41 emu g^{-1}, respectively. The mag-Nb-CST particles after washing could still be easily separated from suspension using a NdFeB-type permanent magnet within only 1 min (inset in Fig. 3), though the magnetic property decreased after removal of the surficial Fe_3O_4.

3.2. Study on adsorption behaviors

It is known that pH has significant influence on adsorption of metal ions. Adsorption performance for Sr^{2+} and Cs^+ were studied with initial pH in the range of 2.00–13.00. The q_e – pH curves are shown in Fig. 4. Adsorption quantity of mag-Nb-CST for Sr^{2+} and Cs^+ was significantly dependent on the initial pH value of solution. The adsorption quantity for Cs^+ increased with the increase of pH value, and reached the maximum of 9.61 mg g^{-1} at pH 4.00. When pH was higher than 4.00, the adsorption quantity decreased with the increase of pH, to the contrary. However, the dependence of adsorption for Sr^{2+} on pH was completely opposite to that of Cs^+. The best condition of adsorption for Sr^{2+} was at pH 11.00, while there was almost no adsorption at pH 4.00. The dependence of adsorption for Sr^{2+} and Cs^+, as well as their

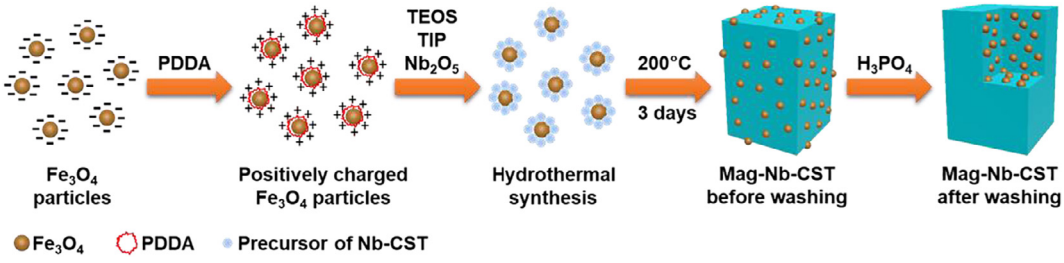

Scheme 1. Schematic illustration for the synthesis of mag-Nb-CST.

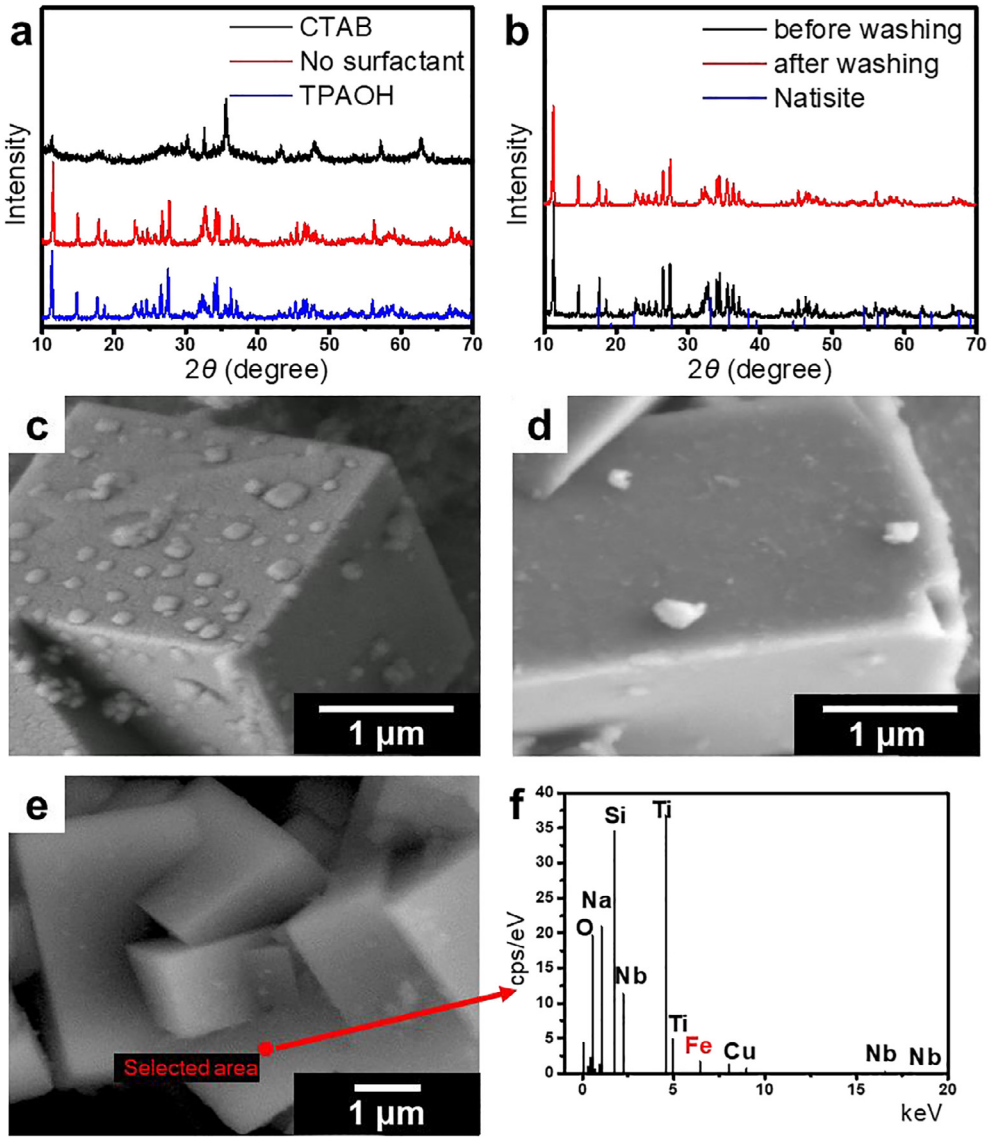

Fig. 2. XRD spectra of (a) products synthesized using different surfactants, (b) mag-Nb-CST synthesized using PDDA before and after washing, the blue lines are the indexed peaks from ICDD PDF 00-29-1279 (natisite). SEM images of (c) mag-Nb-CST before washing, (d) and (e) mag-Nb-CST after washing. (f) EDS of selected area on mag-Nb-CST after washing. (For interpretation of the references to colour in this figure legend, the reader is referred to the web version of this article.)

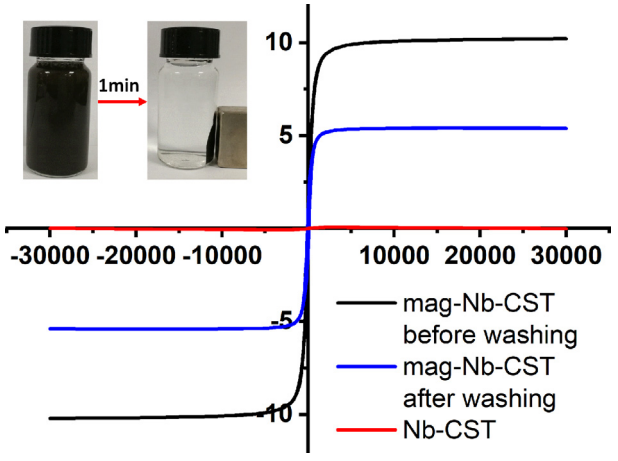

Fig. 3. Magnetization curves of Nb-CST and mag-Nb-CST before and after washing at room temperature. (Inset: attraction of mag-Nb-CST after washing by NdFeB-type permanent magnet).

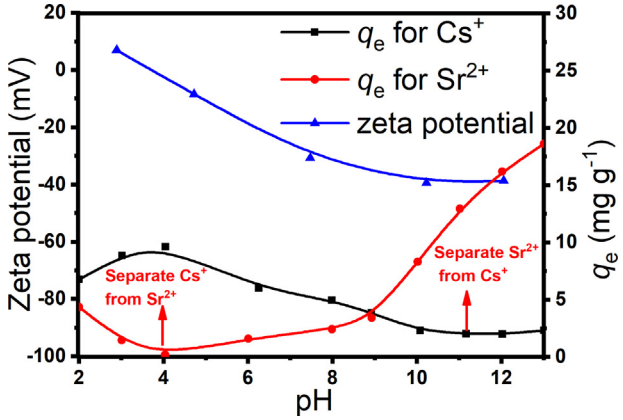

Fig. 4. Effect of pH on zeta potential of mag-Nb-CST and adsorption quantities of Sr^{2+} and Cs^+ on mag-Nb-CST. (Both of the initial concentrations of Sr^{2+} and Cs^+ were 100 ng mL^{-1}; the concentration of mag-Nb-CST was 0.005 g L^{-1}.)

differences, is thought to be caused by the comprehensive effects of pH. On one hand, pH can affect the protonation of silicotitanate. Higher protonation degree of mag-Nb-CST, resulted from lower pH, benefits adsorption of Cs^+ [18]. High protonation degree may also be conducive to the adsorption of strontium. On the other hand, zeta potential of mag-Nb-CST increases with the decrease in pH, and eventually turns into positive at pH below 3.00 (Fig. 4). As a result, electrostatic attraction between mag-Nb-CST and metal cations decreases, and turns into electrostatic repulsion at pH below 3.00, which is disadvantageous to the adsorption of both Sr^{2+} and Cs^+. The effect of zeta potential might be greater than that of protonation on Cs^+ uptake at pH below 4, while the effect of protonation takes the dominating position at pH above 4. The situation for Sr^{2+} is just the opposite. In addition, some species of strontium like $Sr(OH)^+$ and $Sr(OH)_2$ [31,32], conducive to adsorption, are formed at high pH [33], while cesium is always a monovalent cation from acidic to alkaline conditions. Thus, the adsorption quantity of Sr^{2+} has a rapid increase at pH above 9. The differences in the best condition of adsorption for Sr^{2+} and Cs^+ on mag-Nb-CST may open up a new route to separate Sr^{2+}/Cs^+ from each other by the adjustment of pH, which will be discussed in detail below.

Adsorption rate is another important parameter in evaluation of the performance of adsorbent. Adsorption kinetics of Sr^{2+} and Cs^+ was studied at pH 11.00 and 4.00, respectively. Relationship between adsorption quantity of metal ions and contact time is shown in Fig. 5a. The adsorption of Sr^{2+} and Cs^+ on mag-Nb-CST reached the equilibrium within 480 and 180 min, while the equilibrium adsorption quantities of Sr^{2+} and Cs^+ were 12.92 and 9.81 mg g^{-1} (0.29 and 0.07 meq g^{-1}) respectively. The adsorption kinetics of Sr^{2+} and Cs^+ on mag-Nb-CST is fitted by pseudo-first-order and pseudo-second-order kinetics model. The linear forms of the pseudo-first-order and pseudo-second-order model are given by Eq. (5) and Eq. (6):

$$\ln(q_e - q_t) = \ln q_e - k_1 \times t \tag{5}$$

$$\frac{t}{q_t} = \frac{1}{k_2 \times q_e^{\,2}} + \frac{t}{q_e} \tag{6}$$

where q_t (mg g^{-1}) and q_e (mg g^{-1}) are the adsorbed quantity of Sr^{2+} and Cs^+ ions at time t (min) and at equilibrium time respectively, k_1 (min^{-1}) and k_2 (g mg^{-1} min^{-1}) are the pseudo-first-order and the pseudo-second-order adsorption rate constants, respectively.

The linear fitting results of pseudo-first-order and pseudo-second-order kinetic models are listed in Table 1, and the fitting curves are shown in Fig. 5b and c. The determination coefficients (R2) in pseudo-second-order model are larger than those in the pseudo-first-order model, suggesting that adsorption of both Sr^{2+} and Cs^+ can be described by pseudo-second-order kinetics. The equilibrium adsorption capacities Sr^{2+} and Cs^+ on mag-Nb-CST calculated by pseudo-second-order model are 13.14 and 9.84 mg g^{-1}, respectively, which are in good agreement with the experimental data. The results reveal that the adsorption rates are depended on the concentrations of both metal ions and mag-Nb-CST.

Table 1
Kinetic parameters of Sr^{2+} and Cs^+ adsorption on mag-Nb-CST obtained from fitting by pseudo-first-order and pseudo-second-order models.

	Pseudo-first-order			Pseudo-second-order		
	q_e (mg g^{-1})	k_1 (min^{-1})	R^2	q_e (mg g^{-1})	k_2 (g mg^{-1} min^{-1})	R^2
Sr^{2+}	3.09	−0.0047	0.694	13.14	0.012	0.9994
Cs^+	0.68	−0.0030	0.299	9.84	0.014	0.9999

Table 2
Parameters for adsorption isotherms of Sr^{2+} and Cs^+ fitted by Langmuir equation and Freundlich equation.

	Langmuir model			Freundlich model		
	q_{max} (mg g^{-1})	K_L (L g^{-1})	R^2	K_F (mg^{1-n} L^n g^{-1})	n	R^2
Sr^{2+}	14.38	0.743	0.984	4.963	0.191	0.802
Cs^+	11.18	1.486	0.987	3.271	0.201	0.894

According to the adsorption kinetics, there are some significant differences in the adsorption of Sr^{2+} and Cs^+. The difference in charge normalized equilibrium adsorption quantities might be due to the following two aspects. On one hand, adsorption isotherms of Sr^{2+} and Cs^+ were studied at different pH values, i.e., at pH 11.00 and 4.00, respectively. As mentioned above, species like $Sr(OH)^+$ and $Sr(OH)_2$ [31,32] will be formed at high pH, which may be conducive to adsorption [33], but cesium is always a monovalent cation. On the other hand, it is reported that different exchange sites exist in tunnel type adsorbent like CST [34]. Sr^{2+} and Cs^+ occupy different tunnel sites, i.e., six-membered and eight-membered ring tunnel respectively, in which they have different coordination numbers, 7-coordination for Sr^{2+} and 12-coordination for Cs^+ on Nb-CST [21]. Therefore, the charge normalized equilibrium adsorption quantity of Sr^{2+} is much larger than that of Cs^+. Chitra et al. has compared the adsorption performance of Sr^{2+} and Cs^+ on CST and Nb-CST at pH 9 [35]. They found that the ion exchange capacities of Nb-CST towards Sr^{2+} and Cs^+ were estimated to be 11.8 and 3.2 meq g^{-1} respectively, which had the same trend with our results. As for the different equilibrium time, the adsorption rate constant of Cs^+ is slightly larger than Sr^{2+}, while the equilibrium adsorption quantity of Cs^+ is also smaller than Sr^{2+}, leading to a shorter equilibrium time of Cs^+ adsorption.

Adsorption equilibrium isotherm demonstrates how the metal ions distribute between the liquid and solid phases when the adsorption process reaches equilibrium [36]. The adsorption isotherms of Sr^{2+} and Cs^+ on mag-Nb-CST were studied with the initial concentrations varying from 20 to 700 ng mL^{-1} at pH 11.00 for Sr^{2+}, and at pH 4.00 for Cs^+. The data is fitted by Langmuir (Eq. (7)) and Freundlich (Eq. (8)) models, whose isotherms can be represented by the following

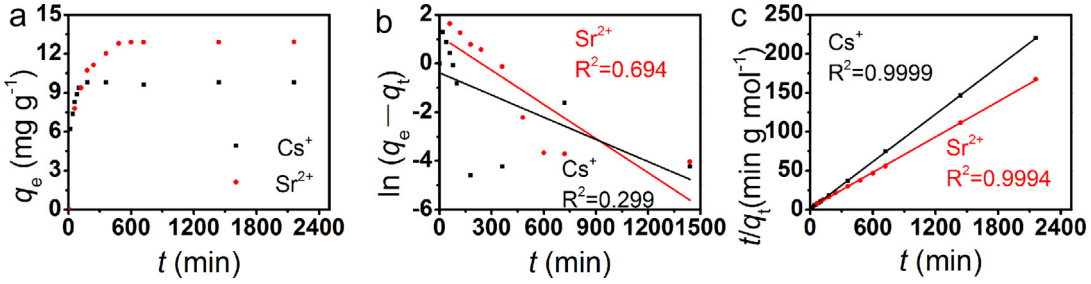

Fig. 5. (a) Effect of contact time on Sr^{2+} and Cs^+ adsorption quantities onto mag-Nb-CST, linear fitting plots of (b) pseudo-first-order adsorption kinetics and (c) pseudo-second-order adsorption kinetics of Sr^{2+} and Cs^+ on the adsorbents. (The initial concentrations of Sr^{2+} and Cs^+ were 100 ng mL^{-1}; the concentration of mag-Nb-CST was 0.005 g L^{-1}.)

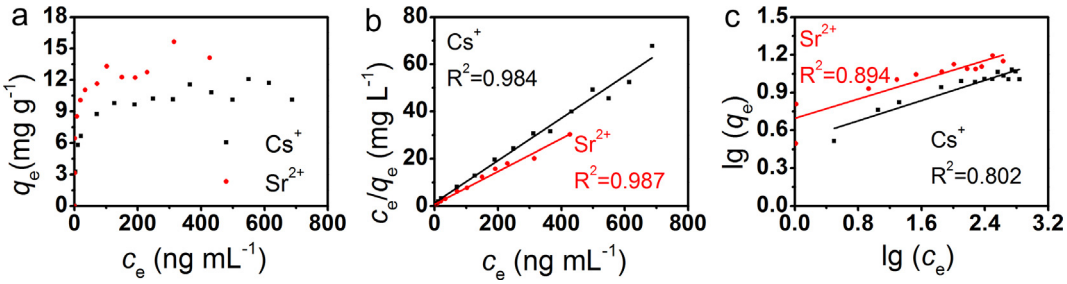

Fig. 6. Adsorption isotherms of (a) Sr^{2+} and Cs^+ onto mag-Nb-CST, linear fitting plots by (b) Langmuir model and (c) Freundlich model. (The initial concentrations of Sr^{2+} varied from 20 to 700 ng mL^{-1} at pH 11.00 and Cs^+ varied from 20 to 750 ng mL^{-1} at pH 4.00; the concentration of mag-Nb-CST was 0.005 g L^{-1}.)

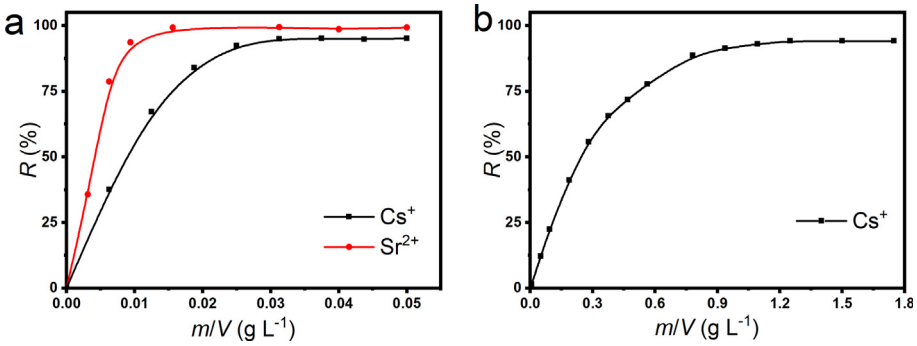

Fig. 7. Removal efficiencies of (a) Sr^{2+} in strontium chloride solution at pH 11.00, Cs^+ in cesium chloride solution at pH 4.00, (b) and Cs^+ in seawater, as a function of the concentration of mag-Nb-CST. (Both of the initial concentrations of Sr^{2+} and Cs^+ were 100 ng mL^{-1}; the concentrations of mag-Nb-CST varied from 0.003 to 1.8 g L^{-1}.)

Table 3
The K_d of Sr^{2+} and Cs^+ on different adsorbents.

Adsorbent	Name	K_d (mL g^{-1})		Reference
		Cs^+	Sr^{2+}	
Titanosilicate	TS88-3	8×10^4	4.5×10^4	[38]
	TAM-5	3×10^4	4×10^3	[39]
	ETS-10	1.6×10^3	–	[40]
	TiSi(p)	–	4×10^4	[41]
	STS	2.2×10^5	2×10^5	[32]
	NaTS	6.5×10^4	1×10^6	[42]
	mag-Nb-CST	5.94×10^5	8.73×10^6	This work
Hexacyanoferrate	$K_{1.34}Ni_{0.33}$[NiFe(CN)$_6$]	1×10^6	–	[43]
	$Fe_3O_4/SiO_2/K_{4y}Ti_x$[Fe(CN)$_6$]	1.25×10^5	–	[44]
	$K_2CoFe(CN)_6 \cdot 1H_2O$	1×10^5	–	[45]
	K_2Zn_3[Fe(CN)$_6$]$_2 \cdot nH_2O$	–	2.3×10^3	[46]
	KCuHCF	1.62×10^5	–	[1]
Layered sulfide	KMS1	1.87×10^3	4.5×10^5	[47]
	KMS1	2×10^4	–	[48]
	KMS2	7.1×10^3	2.1×10^4	[49]
	KTS3	5.5×10^4	3.9×10^5	[50]
Vanadosilicate	Na_xCs_y-SGU-4	1.3×10^5	–	[51]
	ZMTVS	4.0×10^2	2.0×10^2	[52]

equations [37]:

$$\frac{c_e}{q_e} = \frac{c_e}{q_{max}} + \frac{1}{K_L} \quad (7)$$

$$\lg q_e = \lg K_F + n \times \lg c_e \quad (8)$$

where q_{max} (mg g^{-1}) and q_e (mg g^{-1}) are the maximum adsorption quantity and the equilibrium adsorption quantity respectively, c_e (ng mL^{-1}) is the equilibrium concentration in the filtrate, K_L (L g^{-1}) is the Langmuir adsorption equilibrium constant, K_F (mg^{1-n} L^n g^{-1}) and n are the Freundlich adsorption equilibrium constants.

The fitting results in Table 2 and the fitting curves in Fig. 6b and c show that the R^2 in Langmuir fitting of both Sr^{2+} and Cs^+ are larger than those of Freundlich fitting, suggesting the monolayer adsorption of Sr^{2+} and Cs^+ on mag-Nb-CST. The theoretical maximum adsorption capacity for Sr^{2+} on mag-Nb-CST is 14.38 mg g^{-1} (pH = 11), while it is 11.18 mg g^{-1} for Cs^+ (pH = 4), which were calculated based on Langmuir equation.

To determine the best application condition, the studies on removal efficiency for Sr^{2+} and Cs^+ in aqueous solutions were performed separately, at different adsorbent concentrations (m/V) varying from 0.003 to 1.750 g L^{-1}. The removal efficiency for Sr^{2+} reached a maximum of 99.27% when the concentration of adsorbent (m/V) was higher than 0.015 g L^{-1} ($K_d = 8.73 \times 10^6$ mL g^{-1}) at pH 11.00 (Fig. 7a). For Cs^+, it reached a maximum of 94.89% when the

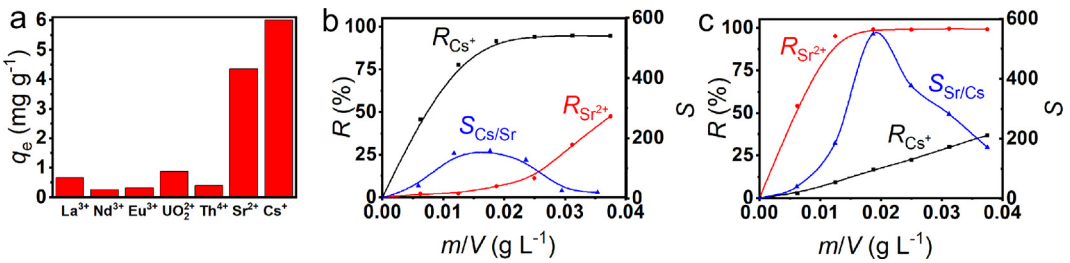

Fig. 8. (a) Adsorption quantities of different cations on mag-Nb-CST. Removal efficiencies of Sr^{2+} and Cs^+ by mag-Nb-CST in a mixture of strontium chloride and cesium chloride solution, and selectivity coefficients between Sr^{2+} and Cs^+ at pH (b) 4.00 and (c) 11.00. (The initial concentrations of La(III), Nd(III), Eu(III), U(VI), Th(IV), Sr(II) and Cs(I) were all 100 ng mL^{-1}; the concentrations of mag-Nb-CST varied from 0.003 to 0.0375 g L^{-1}.)

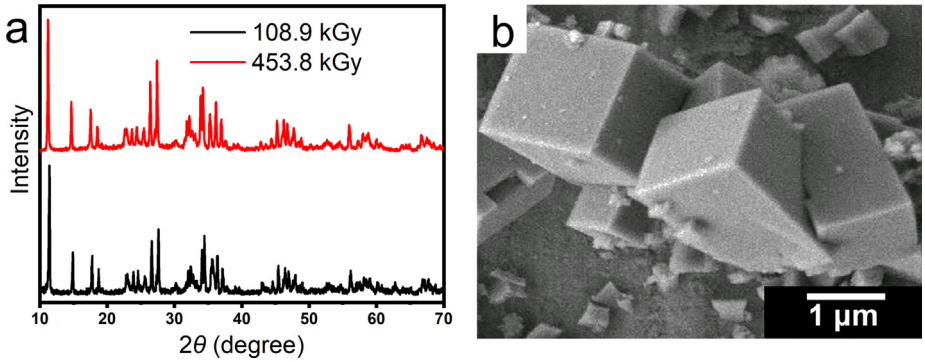

Fig. 9. (a) XRD patterns of mag-Nb-CST irradiated with absorbed doses of 108.9 and 435.8 kGy, (b) SEM image of mag-Nb-CST irradiated with an absorbed dose of 435.8 kGy.

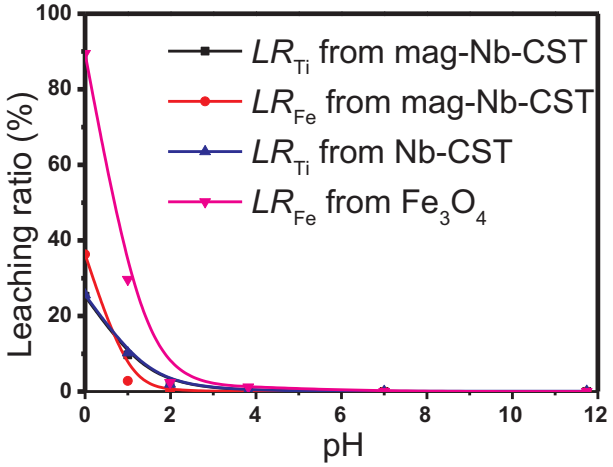

Fig. 10. Leaching ratios of Fe and Ti from mag-Nb-CST, Nb-CST, and Fe_3O_4, in solution of different pH.

concentration of adsorbent was higher than 0.031 g L^{-1} (K_d = 5.94 × 10^5 mL g^{-1}) at pH 4.00 (Fig. 7a). Even in real seawater, though higher pH of seawater and competitive adsorption of alkali metal cations like Na^+ and K^+ were unfavorable to the adsorption of Cs^+ [21] the removal efficiency for Cs^+ at ppb level could still reach as high as 94.19%, which was almost the same as that in pure water, when the concentration of adsorbent was above 1.25 g L^{-1} (K_d = 1.30 × 10^4 mL g^{-1}) (Fig. 7b). The K_d values of adsorption for Sr^{2+} and Cs^+ under different conditions are shown in Fig. S1. We have also investigated the K_d (mL g^{-1}) of Sr^{2+} and Cs^+ on different adsorbents, which is listed in Table 3. Our mag-Nb-CST has an excellent adsorption performance for Sr^{2+} and Cs^+, compared with some previously reported adsorbents.

Some lanthanides and actinides exist in radioactive wastes, whose competitive adsorption may affect the adsorbent performance. Therefore, the adsorption selectivity of Sr^{2+} and Cs^+ over La^{3+}, Nd^{3+}, Eu^{3+}, $UO_2{}^{2+}$, and Th^{4+} was also investigated. To avoid the influence of electrostatic attraction, pH value was kept at 2.00 to ensure the mag-Nb-CST was positively charged. The adsorption quantities on mag-Nb-CST were below 1 mg g^{-1} for all the tested lanthanides and actinides, while they were 4.34 and 6.00 mg g^{-1} for Sr^{2+} and Cs^+, respectively. The excellent selectivity of mag-Nb-CST towards Sr^{2+} and Cs^+ makes it a promising adsorbent in the treatment of radioactive liquid wastes (Fig. 8a).

As mentioned above, the best condition for removal of Sr^{2+} and Cs^+ is at pH 11 and pH 4, respectively. Mag-Nb-CST may also achieve the separation of Sr^{2+}/Cs^+ by adjustment of pH. The selectivity between Sr^{2+} and Cs^+ was studied at pH 4.00 and pH 11.00 in a mixture of Sr^{2+} and Cs^+ at different adsorbent concentrations varying from 0.006 to 0.050 g L^{-1}. Selectivity coefficient is used for evaluating the selectivity between Sr^{2+} and Cs^+, which can be calculated by the follow equations:

$$S_{Sr/Cs} = \frac{K_{d,Sr}}{K_{d,Cs}} \quad (9)$$

$$S_{Cs/Sr} = \frac{K_{d,Cs}}{K_{d,Sr}} \quad (10)$$

where $S_{Sr/Cs}$ is the selectivity coefficients of Sr^{2+} from Cs^+ and $S_{Cs/Sr}$ is the selectivity coefficients of Cs^+ from Sr^{2+}, $K_{d,Sr}$ and $K_{d,Cs}$ are distribution coefficient of Sr^{2+} and Cs^+, respectively. As shown in Fig. 8b and c, $S_{Cs/Sr}$ turned out to be 5.8–156.9 at pH 4.00, while $S_{Cs/Sr}$ turned out to be 44.6–549.4 at pH 11.00. Both of them reached the maximum value (156.9 for $S_{Cs/Sr}$ and 549.4 for $S_{Cs/Sr}$, respectively) when the adsorbent concentration was 0.019 g L^{-1}. The removal efficiency of Sr^{2+} and Cs^+ could almost reach the maximum at the adsorbent concentration of 0.019 g L^{-1} (shown in Fig. 8b and c), indicating that it was the optimum concentration to separate Sr^{2+}/Cs^+. Thus, the mag-Nb-CST can be applied not only in elimination of Sr^{2+} and Cs^+, but also in separation of them from each other.

3.3. Investigation on stability of mag-Nb-CST

As nuclear waste containing ^{90}Sr and ^{137}Cs is radioactive and strongly acidic in usual, radiation stability and acid-resistance are crucial to the adsorbents. The framework structure of Nb-CST results in the formation of eight membered–ring (8MR) tunnels and six membered-rings (6MR) tunnels. As Sr^{2+} and Cs^+ can enter the tunnel and coordinate with oxygen of the 8MR and 6MR [53], the stability of crystal structure would influence the adsorption capacity of Nb-CST. Mag-Nb-CST was irradiated with a Cobalt-60 γ source, to evaluate the radiation stability of crystal structure. After irradiation of 108.9 and 435.8 kGy, no obvious change was observed in the crystal structure and morphology of mag-Nb-CST (Fig. 9a and b).

It has been reported that CST is dissolved to a certain degree when it is exposed to an acidic solution, resulting in a partial conversion to the anatase form of TiO_2 [54]. Here, acid-resistance of mag-Nb-CST was evaluated by the leaching ratios of Ti and Fe, after dispersing them into solutions at different pH, which was kept at 30 °C for 3 days. Leaching ratio (*LR*) was determined using the following equations:

$$LR = \frac{V_1 \times c_1 \times m_2}{1000 \times m_1 \times c_2 \times V_2} \times 100\% \quad (11)$$

where c_1 (ng mL^{-1}) is the concentration of leached Fe (or Ti) in solutions with different pH measured by ICP-MS, V_1 (mL) and m_1 (g) are the solution volume and solid sample mass used in ICP-MS measurement, respectively. c_2 (μg mL^{-1}) is the concentration of Fe (or Ti) after the sample is dissolved with hydrofluoric acid measured by ICP-OES, V_2 (mL) and m_2 (g) are the solution volume and solid sample mass used in

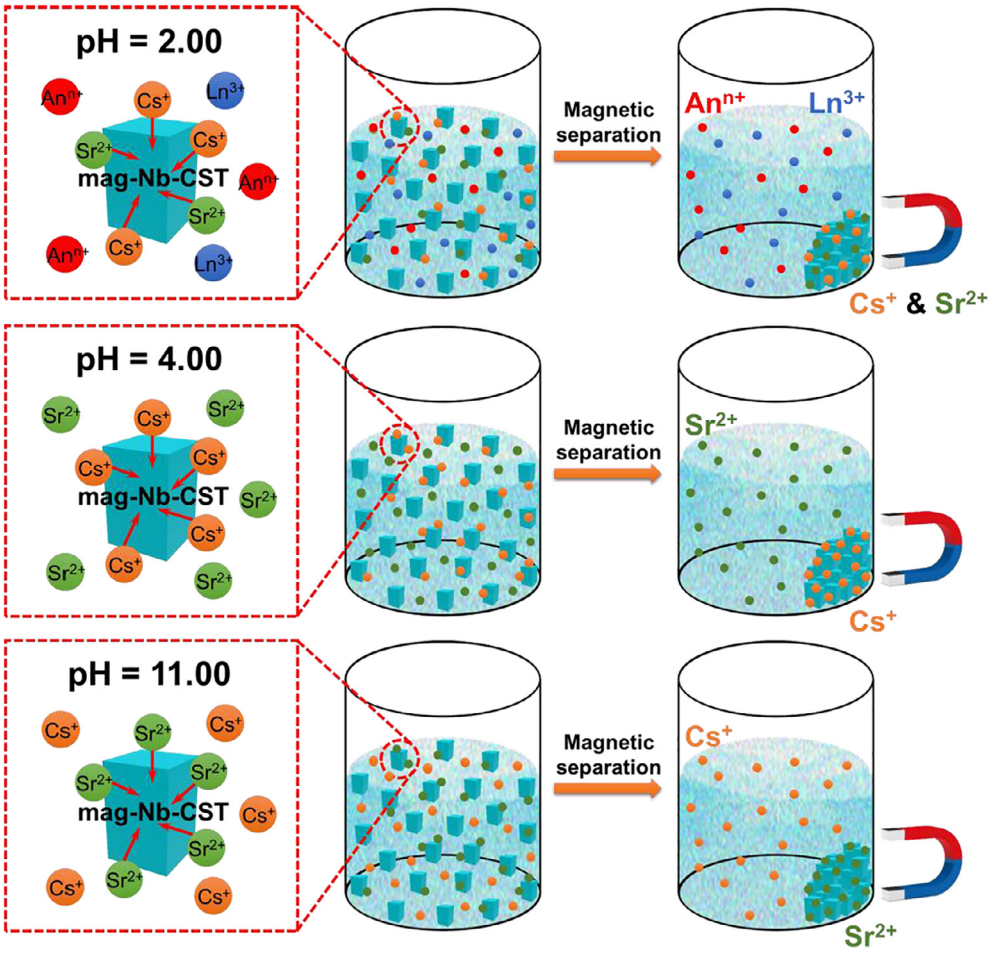

Scheme 2. Schematic illustration for the adsorption and magnetic properties of mag-Nb-CST.

ICP-OES measurement, respectively.

The *LR*-pH curves are shown in Fig. 10. *LR* of Fe from bare Fe_3O_4 and mag-Nb-CST at pH 0 was 89% and 36%, respectively. Evidently, the embedded Fe_3O_4 could be protected by the Nb-CST from acid to some extent. With the increase of pH value, the leaching ratio of both Ti and Fe from mag-Nb-CST decreased sharply. Only less than 2% of Ti and 0.1% of Fe leached out at pH 2.00. When pH value was higher than 4.00, almost no leaching of Ti and Fe were found. In addition, compared with Nb-CST, *LR* of Ti of mag-Nb-CST is nearly the same in the pH range from 0 to 12, indicating that embedding of Fe_3O_4 will not affect the acid-resistance of Nb-CST. The good radiation stability and acid-resistance of mag-Nb-CST make it possible to be applied in acidic medium.

4. Conclusions

Mag-Nb-CST, the hydrothermally synthesized adsorbent with a saturation magnetization value of 5.41 emu g^{-1}, reveals that the magnetic Fe_3O_4 particles are successfully embedded inside the Nb-CST. The possessing of magnetic property makes it possible to conveniently and efficiently separate the adsorbent from the aqueous solutions using an external magnetic field.

Mag-Nb-CST is a rather good adsorbent of Sr^{2+} and Cs^+, which possesses excellent selectivity over various lanthanides and actinides (Scheme. 2). Its maximum adsorption capacity of Sr^{2+} is 14.38 mg g^{-1} at pH 11.00, and that of Cs^+ is 11.18 mg g^{-1} at pH 4.00. It is able to eliminate trace amount of Sr^{2+} and Cs^+ (ng mL^{-1} level). The removal efficiency of Sr^{2+} can be as high as 99.27% at pH 11.00, while that of Cs^+ is 94.89% at pH 4.00. Even in real seawater, the removal efficiency of Cs^+ can reach 94.19%. The significant difference in the pH dependence of adsorption capacity also opens a new route to separate Sr^{2+} from Cs^+ (at pH 11.00) or separate Cs^+ from Sr^{2+} (at pH 4.00) by simply adjusting the pH (Scheme. 2). Thus, mag-Nb-CST could be useful in environmental analytical chemistry, as well as elimination of Sr^{2+} and Cs^+.

In addition, mag-Nb-CST is radiation resistant. Its crystal structure and morphology are stable under γ irradiation with an absorbed dose of 435.8 kGy. Most importantly, it also has very good acid-resistance. In solutions with pH > 2, mag-Nb-CST is quite stable due to the fact that there is almost no leaching of Ti and Fe. These properties are very important in the treatment of radioactive wastes, which often exist in acidic aqueous solutions.

Therefore, it is expected that the as-prepared mag-Nb-CST should have useful applications in the removal of strontium and cesium from radioactive liquid waste and seawater.

Acknowledgements

This work was supported by the National Natural Science Foundation of China (Grant No. 11775214), the China Postdoctoral Science Foundation (2016M592069), the Anhui Provincial Natural Science Foundation (1708085QA21), and the Science Challenging Project (TZ2018004).

Appendix A. Supplementary data

Supplementary data associated with this article can be found, in the online version, at https://doi.org/10.1016/j.cej.2018.06.175.

References

[1] Y. Kim, Y.K. Kim, S. Kim, D. Harbottle, J.W. Lee, Nanostructured potassium copper hexacyanoferrate-cellulose hydrogel for selective and rapid cesium adsorption, Chem. Eng. J. 313 (2017) 1042–1050.

[2] International Atomic Energy Agency, Nuclear Power Reactors in the World, 2017 ed., International Atomic Energy Agency, Austria, 2017.

[3] F. Birol, Key World Energy Statistics, 2016 ed., International Energy Agency, France, 2016.

[4] T.J. Yasunari, A. Stohl, R.S. Hayano, J.F. Burkhart, S. Eckhardt, T. Yasunari, Cesium-137 deposition and contamination of Japanese soils due to the Fukushima nuclear accident, Proc. Natl. Acad. Sci. U.S.A. 108 (2011) 19530–19534.

[5] D. Parajuli, H. Tanaka, Y. Hakuta, K. Minami, S. Fukuda, K. Umeoka, R. Kamimura, Y. Hayashi, M. Ouchi, T. Kawamoto, Dealing with the aftermath of Fukushima Daiichi nuclear accident: decontamination of radioactive cesium enriched ash, Environ. Sci. Technol. 47 (2013) 3800–3806.

[6] Y. Wu, C.P. Lee, H. Mimura, X. Zhang, Y. Wei, Stable solidification of silica-based ammonium molybdophosphate by allophane: application to treatment of radioactive cesium in secondary solid wastes generated from Fukushima, J. Hazard. Mater. 341 (2018) 46–54.

[7] G. Bystrzejewska-Piotrowska, P.L. Urban, Accumulation and translocation of cesium-137 in onion plants (Allium cepa), Environ. Exp. Bot. 51 (2004) 3–7.

[8] B. Mosquera, C. Carvalho, R. Veiga, L. Mangia, R. Anjos, ^{137}Cs distribution in tropical fruit trees after soil contamination, Environ. Exp. Bot. 55 (2006) 273–281.

[9] G. Zibold, E. Klemt, Ecological half-times of ^{137}Cs and ^{90}Sr in forest and freshwater ecosystems, Radioprotection 40 (2005) S497–S502.

[10] T. Watanabe, N. Tsuchiya, Y. Oura, M. Ebihara, C. Inoue, N. Hirano, R. Yamada, S.I. Yamasaki, A. Okamoto, F.W. Nara, Distribution of artificial radionuclides (^{110m}Ag, ^{129m}Te, ^{134}Cs, ^{137}Cs) in surface soils from Miyagi Prefecture, northeast Japan, following the 2011 Fukushima Daiichi nuclear power plant accident, Geochem. J. 46 (2012) (2011) 279–285.

[11] B. Rosoff, S.H. Cohn, H. Spencer, I. Cesium-137 metabolism in man, Radiat. Res. 19 (1963) 643–654.

[12] S.C. Jang, S.B. Hong, H.M. Yang, K.W. Lee, J.K. Moon, B.K. Seo, Y.S. Huh, C. Roh, Removal of radioactive cesium using Prussian blue magnetic nanoparticles, Nanomaterials 4 (2014) 894–901.

[13] S. Fetter, E. Cheng, F. Mann, Long-term radioactivity in fusion reactors, Fusion Eng. Des. 6 (1988) 123–130.

[14] S. Chegrouche, A. Mellah, M. Barkat, Removal of strontium from aqueous solutions by adsorption onto activated carbon: kinetic and thermodynamic studies, Desalination 235 (2009) 306–318.

[15] X.M. Zheng, J.F. Dou, M. Xia, A.Z. Ding, Ammonium-pillared montmorillonite-$CoFe_2O_4$ composite caged in calcium alginate beads for the removal of Cs^+ from wastewater, Carbohydr. Polym. 167 (2017) 306–316.

[16] J.E. Miller, N.E. Brown, Development and Properties of Crystalline Silicotitanate (CST) Ion Exchangers for Radioactive Waste Applications, Sandia National Laboratories, Albuquerque, NM (United States), 1997.

[17] R.G. Anthony, R.G. Dosch, D. Gu, C. Philip, Use of silicotitanates for removing cesium and strontium from defense waste, Ind. Eng. Chem. Res. 33 (1994) 2702–2705.

[18] D.M. Poojary, A.I. Bortun, L.N. Bortun, A. Clearfield, Structural studies on the ion-exchanged phases of a porous titanosilicate, $Na_2Ti_2O_3SiO_4{\cdot}2H_2O$, Inorg. Chem. 35 (1996) 6131–6139.

[19] J. Rocha, P. Brandão, Z. Lin, A. Kharlamov, M.W. Anderson, Novel microporous titanium–niobium–silicates with the structure of nenadkevichite, Chem. Commun. 669–670 (1996).

[20] J. Rocha, P. Brandao, Z. Lin, A. Esculcas, A. Ferreira, M.W. Anderson, Synthesis and structural studies of microporous titanium–niobium–silicates with the structure of nenadkevichite, J. Phys. Chem. 100 (1996) 14978–14983.

[21] A. Tripathi, D.G. Medvedev, M. Nyman, A. Clearfield, Selectivity for Cs and Sr in Nb-substituted titanosilicate with sitinakite topology, J. Solid State Chem. 175 (2003) 72–83.

[22] T.Y. Chen, Immobilisation of Caesium from Crystalline Silicotitanate by Hot Isostatic Pressing, University of Birmingham, 2012.

[23] N.R. Mann, T.A. Todd, Removal of cesium from acidic radioactive tank waste by using IONSIV IE-911, Sep. Sci. Technol. 39 (2005) 2351–2371.

[24] N. Limchoowong, P. Sricharoen, Y. Areerob, P. Nuengmatcha, T. Sripakdee, S. Techawongstien, S. Chanthai, Preconcentration and trace determination of copper (II) in Thai food recipes using Fe_3O_4@Chi-GQDs nanocomposites as a new magnetic adsorbent, Food Chem. 230 (2017) 388–397.

[25] Y. Zhu, W. Wang, H. Zhang, X. Ye, Z. Wu, A. Wang, Fast and high-capacity adsorption of Rb^+ and Cs^+ onto recyclable magnetic porous spheres, Chem. Eng. J. 327 (2017) 982–991.

[26] W. Mu, Q. Yu, X. Li, H. Wei, Y. Jian, Efficient removal of Cs^+ and Sr^{2+} from aqueous solution using hierarchically structured hexagonal tungsten trioxide coated Fe_3O_4, Chem. Eng. J. 319 (2017) 170–178.

[27] H. Yang, H. Yu, J. Sun, J. Liu, J. Xia, J. Fang, Y. Li, F. Qu, A. Song, T. Wu, Facile synthesis of mesoporous magnetic AMP polyhedric composites for rapid and highly efficient separation of Cs^+ from water, Chem. Eng. J. 317 (2017) 533–543.

[28] S.M. Husnain, W. Um, Y.Y. Chang, Y.S. Chang, Recyclable superparamagnetic adsorbent based on mesoporous carbon for sequestration of radioactive cesium, Chem. Eng. J. 308 (2017) 798–808.

[29] C. Hou, Y. Wang, H. Zhu, H. Wei, Construction of enzyme immobilization system through metal-polyphenol assisted Fe_3O_4/chitosan hybrid microcapsules, Chem. Eng. J. 283 (2016) 397–403.

[30] L. Wang, J. Bao, L. Wang, F. Zhang, Y. Li, One-pot synthesis and bioapplication of amine-functionalized magnetite nanoparticles and hollow nanospheres, Chem. Eur. J. 12 (2006) 6341–6347.

[31] N.A. Lange, J.A. Dean, Lange's Handbook of Chemistry, McGraw-Hill, 1979.

[32] S. Solbrå, N. Allison, S. Waite, S.V. Mikhalovsky, A.I. Bortun, L.N. Bortun, A. Clearfield, Cesium and strontium ion exchange on the framework titanium silicate $M_2Ti_2O_3SiO_4{\cdot}nH_2O$ (M = H, Na), Environ. Sci. Technol. 35 (2001) 626–629.

[33] T. Shvareva, Design and Properties of Novel Uranium-containing Layered and Framework Materials, Ph.D Thesis Auburn University, 2006.

[34] A. Clearfield, Structure and ion exchange properties of tunnel type titanium silicates, Solid. State Sci. 3 (2001) 103–112.

[35] S. Chitra, S. Viswanathan, S. Rao, P. Sinha, Uptake of cesium and strontium by crystalline silicotitanates from radioactive wastes, J. Radioanal. Nucl. Chem. 287 (2011) 955–960.

[36] S.W. Chen, B.L. Guo, Y.L. Wang, Y. Li, L.J. Song, Study on sorption of U(VI) onto ordered mesoporous silicas, J. Radioanal. Nucl. Chem. 295 (2012) 1435–1442.

[37] C.L. Chen, X.L. Li, X.K. Wang, Application of oxidized multi-wall carbon nanotubes for Th(IV) adsorption, Radiochim. Acta 95 (2007) 261–266.

[38] A.I. Bortun, L.N. Bortun, A. Clearfield, Ion exchange properties of a cesium ion selective titanosilicate, Solvent Extr. Ion. Exc. 14 (1996) 341–354.

[39] R. Anthony, C. Philip, R. Dosch, Selective adsorption and ion exchange of metal cations and anions with silico-titanates and layered titanates, Waste Manage. 13 (1993) 503–512.

[40] C. Pavel, K. Popa, N. Bilba, A. Cecal, D. Cozma, A. Pui, The sorption of some radiocations on microporous titanosilicate ETS-10, J. Radioanal. Nucl. Chem. 258 (2003) 243–248.

[41] O. Oleksiienko, I. Levchuk, M. Sitarz, S. Meleshevych, V. Strelko, M. Sillanpaa, Removal of strontium (Sr^{2+}) from aqueous solutions with titanosilicates obtained by the sol-gel method, J. Colloid. Interf. Sci. 438 (2015) 159–168.

[42] A. Dyer, M. Pillinger, S. Amin, Ion exchange of caesium and strontium on a titanosilicate analogue of the mineral pharmacosiderite, J. Mater. Chem. 9 (1999) 2481–2487.

[43] C. Michel, Y. Barré, C. de Dieuleveult, A. Grandjean, L. De Windt, Cs ion exchange by a potassium nickel hexacyanoferrate loaded on a granular support, Chem. Eng. Sci. 137 (2015) 904–913.

[44] H. Zhang, X. Zhao, J. Wei, F. Li, Removal of cesium from low-level radioactive wastewaters using magnetic potassium titanium hexacyanoferrate, Chem. Eng. J. 275 (2015) 262–270.

[45] J. Lehto, R. Harjula, J. Wallace, Absorption of cesium on potassium cobalt hexacyanoferrate (II), J. Radioanal. Nucl. Chem. 111 (1987) 297–304.

[46] A. Nilchi, M.R. Hadjmohammadi, S. Rasouli Garmarodi, R. Saberi, Studies on the adsorption behavior of trace amounts of $^{90}Sr^{2+}$, $^{140}La^{3+}$, $^{60}Co^{2+}$, Ni^{2+} and Zr^{4+} cations on synthesized inorganic ion exchangers, J. Hazard. Mater. 167 (2009) 531–535.

[47] M.J. Manos, N. Ding, M.G. Kanatzidis, Layered metal sulfides: exceptionally selective agents for radioactive strontium removal, Proc. Natl. Acad. Sci. U.S.A. 105 (2008) 3696–3699.

[48] M.J. Manos, M.G. Kanatzidis, Highly efficient and rapid Cs^+ uptake by the layered metal sulfide $K_{2x}Mn_xSn_{3-x}S_6$ (KMS-1), J. Am. Chem. Soc. 131 (2009) 6599–6607.

[49] J.L. Mertz, Z.H. Fard, C.D. Malliakas, M.J. Manos, M.G. Kanatzidis, Selective removal of Cs^+, Sr^{2+}, and Ni^{2+} by $K_{2x}Mg_xSn_{3-x}S_6$ (x = 0.5–1) (KMS-2) relevant to nuclear waste remediation, Chem. Mater. 25 (2013) 2116–2127.

[50] D. Sarma, C.D. Malliakas, K.S. Subrahmanyam, S.M. Islam, M.G. Kanatzidis, $K_{2x}Sn_{4-x}S_{8-x}$ (x = 0.65–1): a new metal sulfide for rapid and selective removal of Cs^+, Sr^{2+} and UO_2^{2+} ions, Chem. Sci. 7 (2016) 1121–1132.

[51] S.J. Datta, W.K. Moon, D.Y. Choi, I.C. Hwang, K.B. Yoon, A novel vanadosilicate with hexadeca-coordinated Cs^+ ions as a highly effective Cs^+ remover, Angew. Chem. 53 (2014) 7203–7208.

[52] F.M. Zonoz, S.J. Ahmadi, S.A. Nosrati, M.G. Maragheh, Preparation and characterization of zirconium (IV) molybdo tungsto vanado silicate as a novel inorganic ion exchanger in sorption of radionuclides, J. Hazard. Mater. 169 (2009) 808–812.

[53] A. Tripathi, D.G. Medvedev, A. Clearfield, The crystal structures of strontium exchanged sodium titanosilicates in relation to selectivity for nuclear waste treatment, J. Solid State Chem. 178 (2005) 253–261.

[54] B. Yu, J. Chen, C. Song, Crystalline silicotitanate: a new type of ion exchanger for Cs removal from liquid waste, J. Met. Sci. Technol. 18 (2002) 206–210.